Nano Energy 51 (2018) 728–735

Contents lists available at ScienceDirect

Nano Energy

journal homepage: www.elsevier.com/locate/nanoen

Full paper

Study of long-term biocompatibility and bio-safety of implantable nanogenerators

Jun Li[a], Lei Kang[b,c], Yanhao Yu[a], Yin Long[a], Justin J. Jeffery[f], Weibo Cai[b,d,e,f,*], Xudong Wang[a,*]

[a] Department of Materials Science and Engineering, University of Wisconsin-Madison, WI 53706, USA
[b] Department of Radiology, University of Wisconsin-Madison, WI 53705, USA
[c] Department of Nuclear Medicine, Peking University First Hospital, Beijing 100034, China
[d] Department of Medical Physics, University of Wisconsin-Madison, Madison, WI 53705, USA
[e] School of Pharmacy, University of Wisconsin-Madison, Madison, WI 53705, USA
[f] University of Wisconsin Carbone Cancer Center, Madison, WI, 53705, USA

ARTICLE INFO

Keywords:
Implantable Nanogenerator
Biocompatibility
In Vivo imaging
PVDF
Biomechanical energy harvesting

ABSTRACT

Implantable nanogenerator (i-NG) has shown great promises for enabling self-powered implantable medical devices (IMDs). One essential requirement for practical i-NG applications is its long-term bio-compatibility and bio-safety. This paper presents a systematic study of polydimethylsiloxane (PDMS) and PDMS/Parylene-C packaged polyvinylidene fluoride (PVDF) NGs implanted inside female ICR (Institute of Cancer Research) mice for up to six months. The PVDF NG had a stable *in vitro* output of 0.3 V when bended for 7200 cycles and an *in vivo* output of 0.1 V under stretching. Multiple advanced imaging techniques, including computed tomography (CT), ultrasound, and photoacoustic were used to characterize the embedded i-NGs *in vivo*. The i-NGs kept excellent adhesion to the adjacent muscle surface, and exhibited stable electrical output during the entire examine period. No signs of toxicity or incompatibility were observed from the surrounding tissues, as well as from the whole body functions by pathological analyses and blood and serum test. The PDMS package was also able to effectively insulate the i-NG in biological environment with negligible stray currents at a pA scale. This series of *in-vivo* and *in-vitro* studies confirmed the biological feasibility of using i-NG *in vivo* for biomechanical energy harvesting.

1. Introduction

During the last ten years, nanogenerator (NG), a device that harvests micro- and nanoscale mechanical energy and converts it into electricity, has been rapidly advanced from a conceptual design to a practical technology for efficient mechanical energy harvesting from the ambient environment [1–6]. The simple configuration, high efficiency, decent electrical output and good flexibility have endowed NGs a great potential for powering implantable medical devices. Since the first demonstration of ZnO nanowire-based implantable NG (i-NG) in 2010 [7], i-NGs has been consistently investigated and developed as a self-sustainable implantable power source and for real-time healthcare monitoring [8,9]. For example, flexible NG based on polyvinylidene fluoride (PVDF) microbelts with tunable thickness was developed to harvest energy from low-speed air flow, and demonstrated an open-circuit voltage of ~ 0.5 V driven by respiration [10]. The open-circuit voltage of a NG is typically defined as the voltage measured between the two NG electrodes when there is no load connected in between. A maximum output power (defined as the electrical energy generated per unit time) of 12 μW was achieved on a 100 kΩ load. A flexible and implanted NG based on lead zirconate titanate (PZT) nanoribbons was developed to affix on the heart of bovine and an output open-circuit voltage up to 4 V was generated upon heart beating [11]. Kim *et al.* reported a high performance (1-x)$Pb(Mg_{1/3}Nb_{2/3})O_3$-(x)$Pb(Zr,Ti)O_3$ (PMN-PZT) i-NG with an open-circuit voltage of 17.8 V from the contraction and relaxation of a porcine heart [12]. These recent developments of i-NG showed consistent > 3 V output voltage from regular body functions, which was sufficient to power small implantable medical devices (IMDs), such as pacemakers, cardiac defibrillator, and hearing aid [13,14]. In addition, applying i-NG as an active sensor for real-time biomedical monitoring has also been attracting growing interests. A number of physiological and pathological behaviors such as respiration, heartbeat and blood pressure, could be accurately and continuously monitored by interpreting and recording the voltage signals from specially-designed i-NG systems, providing excellent sensitivity, and spatial and time resolution [15–17]. Most recently,

* Corresponding authors.
E-mail addresses: WCai@uwhealth.org (W. Cai), xudong.wang@wisc.edu (X. Wang).

https://doi.org/10.1016/j.nanoen.2018.07.008
Received 28 May 2018; Received in revised form 1 July 2018; Accepted 5 July 2018
Available online 06 July 2018

intriguing interactions between i-NG and cell activities were further discovered. The periodic biphasic pulse-like electrical signals generated from NG were found capable of accelerating cellular proliferation, adjusting cellular orientation, stimulating cellular motility and inducing intracellular calcium transients [18–20].

One of the most essential requirements for i-NG development is the long-term bio-compatibility and bio-safety. Earlier work on NG development has demonstrated extensively long life span of the piezoelectric functional components owing to the nanoscale size, which offers much higher flexibility and fractural tolerance compared to the bulk morphology [21–23]. Even ceramics based NGs could operate for more than 100,000 straining cycles without observable performance degradation [9]. Our previous work also showed a continuous and steady operation of PVDF-based NGs for more than 1.5×10^8 straining cycles [24]. Although such long straining cycles are sufficient for *in vivo* operation of NG for 5–10 years in theory, long-term assessment of i-NG in biological systems has not been investigated. Recent work has demonstrated the biocompatibility and safe operations of piezoelectric i-NG *in vivo* for a few days, such as $LiNbO_3$-doped (K,Na)NbO_3(KNN) thin-film-based i-NGs [25]. Nevertheless, since most IMDs are designed to have years-long life span, it is necessary for i-NGs to have at least the same operation lifetime. Meanwhile, considering the potential risks of immune reactions and infections over a long period of time, biological influence of i-NG also needs to be fully evaluated to justify their implantation feasibility. To fill the gap and address this critical issue, herein we systematically investigated the long-term bio-compatibility and bio-safety of PVDF-based piezoelectric NGs in female ICR mice, including the stability of materials functionality in biological environment, and NG's influence to biological systems. PVDF was chosen in i-NG design because of their combined merits of good mechanical flexibility and reasonably high piezoelectric coefficients (20–30 pC/N for d_{33} and 16 pC/N for d_{31}), which are critical for implanted devices [26]. Up to six months *in vivo* testing, i-NGs exhibited excellent structural and functional stability over the entire implantation period. Histological, blood and serum examinations also revealed no signs of toxicity or incompatibility. This research confirmed the long-term bio-compatibility of flexible i-NGs and provided the first cornerstone for practical i-NG system implantation.

2. Experimental section

2.1. Fabrication of i-NG

A piezoelectric PVDF film (~ 50 μm in thickness, from Measurement Specialties Inc.) was cut into a 5 mm × 5 mm piece first. A layer of 50 nm gold was deposited on both sides of the PVDF film as electrodes by E-beam Evaporator (CHA-600). Four small holes (~ 0.8 mm in diameter) were drilled by micro drill press at each corner of the PVDF film. Then, a polydimethylsiloxane (PDMS) (Sylgard 184, Tow Corning) solution consisting of pre-mixed elastomer and crosslinker at the ratio of 10–1 was spin coated on both sides of PVDF film with different thickness. The 100 μm PDMS film was coated at the speed of 800 rpm for 60 s; while the 300 μm PDMS film was coated at the speed of 200 rpm for 60 s. Another four small holes (~ 0.8 mm in diameter) were drilled by the small benchtop drill press (DRL-300.00) at each corner of the PDMS film. For PDMF/Parylene-C packaged NGs, the PVDF NG was first encapsulated by PDMS through the same procedure discussed above. Then a 15–20 μm Parylene-C thin film was deposited on both side of the PDMS package using a parylene chemical deposition system (Model 3000 Lab Top, PARA Tech Coating, Inc.). Inside the deposition system, 4 g dimer (Parylene Type “C”, Parylene Coating Service, Inc) was first vaporized at 130 °C and then pyrolyzed at 650 °C and at 15–20 mTorr to form Parylene-C vapor. The vapor went through a post-pyrolysis heater with a temperature of 220 °C and flew into the room temperature deposition chamber (The temperature of deposition chamber was in the range of 25–65 °C). After deposition, four small holes (~ 0.8 mm in diameter) were drilled by the small benchtop drill press at each corner of the PDMS/Parylene C film.

2.2. i-NG characterization

To characterize the piezoelectric output of NG, the leads were first bonded with PVDF films and then the PVDF films with leads were packaged by PDMS. One end of the packaged PVDF film was fixed on a stationary stage, while another end was attached to a moveable stage. Driven by a permanent magnet shaker (LV201, M4-CE), the film was bended and released at a bending radius of 0.63 cm with a controlled frequency. The voltage was recorded by an Agilent DSO1012A oscilloscope. The oscilloscope probes were directly connected to the two electrodes of the NG and no additional load resistant was added in between. When evaluating the piezoelectric performance after implantation, the i-NG was fixed on a flat bench surface. After the device was extracted from the rat hosts at different time frame, the excess PDMS on one side of device was removed and two thin leads were inserted into device to make contacts with either side of PVDF. A force of 6 N (quantified by a Force Gauge HF-500N) was applied to the entire NG surface by a permanent magnet shaker (LV201, M4-CE) at 2 Hz. The frequency was controlled by a function generator (Stanford Research Systems, Model DS345) and the force was tuned by a signal amplifier (Harman/Kardon, A-401). The voltage outputs were recorded by the same oscilloscope setup as descried above. For stray current measurement, a device consisting of gold electrode (5 mm × 5 mm) and PDMS package (200 μm thick) was immersed in a 60 mL 0.9% NaCl saline solutions. A function generator (Stanford Research Systems, Model DS345) connected with 1 MΩ resistor was used to provide a continuous sinusoidal 20 μA current (peak-to-peak) toward electrode to simulate the NG output. A copper electrode was attached to the surface of PDMS package, and the stray current flowing from the copper electrode to the ground was measured periodically by a low noise current preamplifier (Stanford Research Systems, Model SR570).

2.3. PVDF phase characterization

X-ray diffraction patterns of PVDF films were acquired from the Bruker D8 Discovery with Cu Kα radiation.

2.4. Implantation of the NGs

All animal experiments were conducted under a protocol approved by the University of Wisconsin Institutional Animal Care and Use Committee. 4-to-6-week-old female ICR mice (Envigo, New Jersey, USA) were used to investigate the biocompatibility of the NGs post-implantation. Briefly, anesthesia was introduced by inhalation of 5% isoflurane and maintained with 2% isoflurane. Following anesthesia, the mice were placed at the prone position. After the region of lower back was sterilized with iodine and alcohol scrubs for three times, a skin incision of ~ 3 cm was made near the hip joint. The NGs were placed between the epithelial and deep muscle layer and were further fixed on deep muscle layer by diagonal sutures using natural proteinaceous silk fibers. At last, the incision was sutured, then animals were allowed to recover and remained normal activity for up to 6 months.

2.5. In vivo imaging methods for the assessment of NG

Computer tomography (CT), ultrasound, and photoacoustic imaging were performed to evaluate the position and integrity of NGs post-implantation. In brief, for CT imaging, mice were laid at the prone position after anesthesia. CT was scanned using an Inveon microPET/CT scanner (Siemens Medical Solutions, USA) at the 4th, 12th, and 24th week of post-implantation. For photoacoustic imaging, the mice were anesthetized and set on a VisualSonics Vevo2100 LAZR instrument (Fujifilm, Japan). The target region was covered with ultrasonic

coupling gel and imaged using the Visualsonics Vevo LAZER system with an excitation wavelength at 690 nm. Ultrasound imaging was also performed using this VisualSonics Vevo2100 LAZR instrument.

2.6. Safety assessment of NG in mice

Histological analysis, blood and serum test were used for safety assessment of NG in mice at the 2nd, 4th, 12th, and 24th week of post-implantation, respectively. For histological analysis, after animals were euthanized, tissue around NG was collected for histological analysis, containing the skin, superficial muscle, connective tissue, deep muscle and the device on the top of deep muscle layer. The tissue was frozen and sectioned at 10 μm thickness at the vertical direction of skin. Tissue sections were hematoxylin and eosin (H&E) stained for analysis. Assessment of the tissue sections used four criteria including: (1) degree of inflammatory infiltrate; (2) degree of fibrosis; (3) presence of muscle degeneration; and (4) presence and degree of cellular toxicities around NG (*e.g.,* change of cell shape, cellular nucleus, etc). For blood and serum test, orbital whole blood was collected before animals were euthanized. Blood test was performed using an Abaxis VetScan HM5 Hematology Analyzer (Allied Analytic, USA). After the whole blood was centrifuged at a speed of 2000 rpm, serum was collected for urea nitrogen, creatinine, AST, and ALT measurement.

3. Results and discussions

3.1. NG implantation and electrical outputs

PVDF, a ferroelectric polymer with high piezoelectric coefficients (20–30 pC/N for d_{33} and 16 pC/N for d_{31}) and good biocompatibility, has recently been used as the functional material building block for i-NG development [24,27,28]. In this work, PVDF NGs with selected packaging materials were used as a model system to study the biocompatibility. Fig. 1a presents the schematic structure of a packaged PVDF NG. Four small holes were drilled at each corner of the PVDF film to pin the PVDF film tightly with the packaging material. These pin holes were critical to ensure that the strain subjected by the packaging material can be well transmitted to the PVDF film. Two typical biocompatible polymer materials, PDMS and Parylene-C, were selected for packaging. Parylene-C has long been used as the protective coating for medical device. The long-term biocompatibility of PDMS has also been confirmed by several independent studies. (Supplementary Material S2) [29–31] The PDMS packaging layer was spin coated on both sides of the PVDF film with different thicknesses (Fig. S1). The asymmetric thickness of PDMS layer was designed to ensure that the PVDF film was positioned away from the neutral-strain plane during bending. A group of PDMS-packaged PVDF was selected to receive an addition layer of Parylene-C coating. The multilayer packaging was expected to provide enhanced protection against biofluids erosion and electrical leakage. Another four pin holes at each corner were designed for affixing the i-NG to the muscle layer by sutures. The PVDF film remained its β phase after the entire fabrication procedures (Fig. S2) and the piezoelectric output was only slightly reduced (by < 50 mV) after the complete packaging (Fig. S3). The as-fabricated i-NG device was then tested *in vitro* under regular deflection. When bended at a frequency of 2 Hz (to closely represent the actual biomechanical energy stimulations found in biological systems) [32,33], the NG exhibited a consistent peak-to-peak current of ~ 45 nA (Fig. S4) and a voltage of ~ 0.3 V (Fig. 1b) for over 7200 bending cycles (Fig. S5). This stable output confirmed the good piezoelectric behavior of the PVDF film as well as a reasonably high piezoelectric output even under the package of polymer materials.

The surgery steps for i-NG implantation were shown in Fig. 1c. All surgery procedures followed the standard surgery protocol. To prevent infection, the packaged i-NG devices were sterilized before implantation. The lower right back near the hip joint was chosen as the implantation location, where the device could be easily deflected when the mouse moved their lower limbs. At first, an incision of ~ 3 cm was cut down to the level of deep muscle (Fig. 1c-i). Then, the upper connective tissue and superficial muscle layer were detached, and the sterilized i-NG was sutured on the surface of deep muscle to ensure a tight attachment and no relative movements between the i-NG and muscle surface (Fig. 1c-ii). Given that the connective tissue between skin and muscle is easy to remove, therefore, there is plenty room for NG implantation. After implantation, the incision was sutured back to

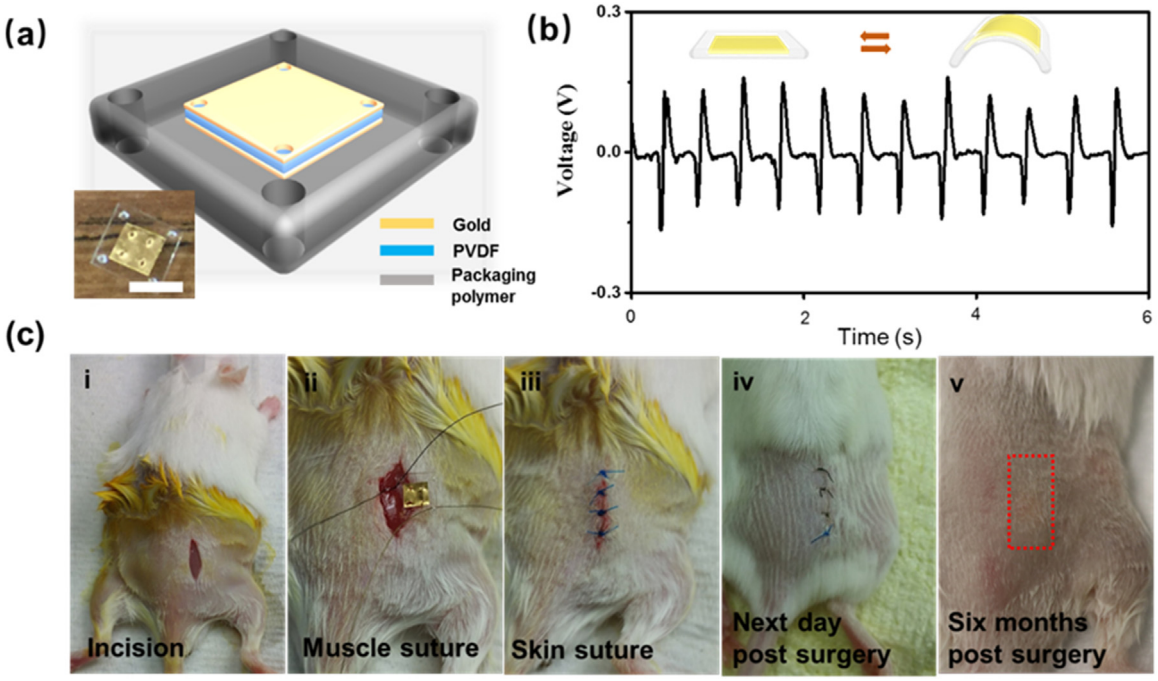

Fig. 1. NG fabrication and implantation. **(a)** Schematic structure of a packaged PVDF i-NG. Inset is a photo of the actual device, where the scale bar is 5 mm. **(b)** In vitro voltage outputs of a packaged PVDF i-NG when deflected at a frequency of 2 Hz. Inset schematically shows deflection direction. **(c)** Digital photos showing the typical surgery process of NG implantation (i)-(iii), and wound healing situations of the implantation area in the next day (iv) and after six months (v) post-surgery.

completely cover the i-NG inside the mouse body (Fig. 1c-iii). After the surgery, the mice behaved normally without any disorder of movement. The wound healed well without any inflammation on the skin one-day post-surgery (Fig. 1c-iv). The skin fully recovered without any scar after 6 months (Fig. 1c-v), and the mouse behaved normally during such a long period time (Supplementary video S1). These results evidenced a successful i-NG implantation, which was critical for long-term biocompatibility and bio-safety study.

Supplementary material related to this article can be found online at doi:10.1016/j.nanoen.2018.07.008.

3.2. *In vivo* study of implantation and biocompatibility

Computed Tomography (CT), Ultrasound and Photoacoustic imaging were utilized to observe *in vivo* characteristics of the implanted NGs. The small-animal CT produces 3-dimensional (3D) x-ray images were based on the information of tissue densities, which were able to reconstruct a high-definition 3D images of animals with a resolution up to 100 μm [34]. Therefore, CT imaging was able to provide a precise monitoring of the suture effectiveness and i-NG's structural integrity inside the mouse body. At the 4th, 12th, and 24th week of post-implantation, the same ICR mice implanted with NGs were scanned by CT. The whole-body 3D projection CT images demonstrated that both i-NGs (packaged with PDMS, and PDMS/Parylene-C) remained at the same region without observable displacements (Fig. 2a). After 24 weeks of implantation, fine structures such as the shape of the i-NG, pin holes, and position of the PVDF layer could still be clearly visualized (Fig. 2b), confirming that there were no observable damages and degradations of the packages on both i-NGs. Transverse CT images showed that i-NGs were located subcutaneously and wrapped tightly by the surrounding tissues without any change of CT density, indicating good interfacial compatibility between device and muscle/tissue (Fig. 2c). These CT images revealed excellent long-term biocompatibility of both PDMS and PDMS/Parylene-C packaged i-NGs.

Photoacoustic imaging combines the high contrast of optical imaging with the high spatial resolution of ultrasound, and is able to show the optical properties of different tissues [35]. In our study, gold electrodes could be detected at the absorption wavelength of ~ 690 nm by photoacoustic imaging. Both PDMS and Parylene-C packaged NGs displayed a “sandwich”-like signal in photoacoustic imaging (Fig. S6). Two long lines with hyper echo represented the upper and bottom encapsulation layers of the i-NG. The short line at the center with hyper echo was high photoacoustic signals from the gold electrodes. While CT scan was impractical to detect the gold electrodes, photoacoustic imaging perfectly revealed the fact that gold electrodes were well protected by the encapsulation.

Ultrasound imaging was then used to obtain real-time observation of the motion of i-NGs in response to muscle movements. Fig. 2d and e show a series of ultrasound images recorded when the ICR mice moved their right lower hip joints. The i-NG exhibited bright contrasts under

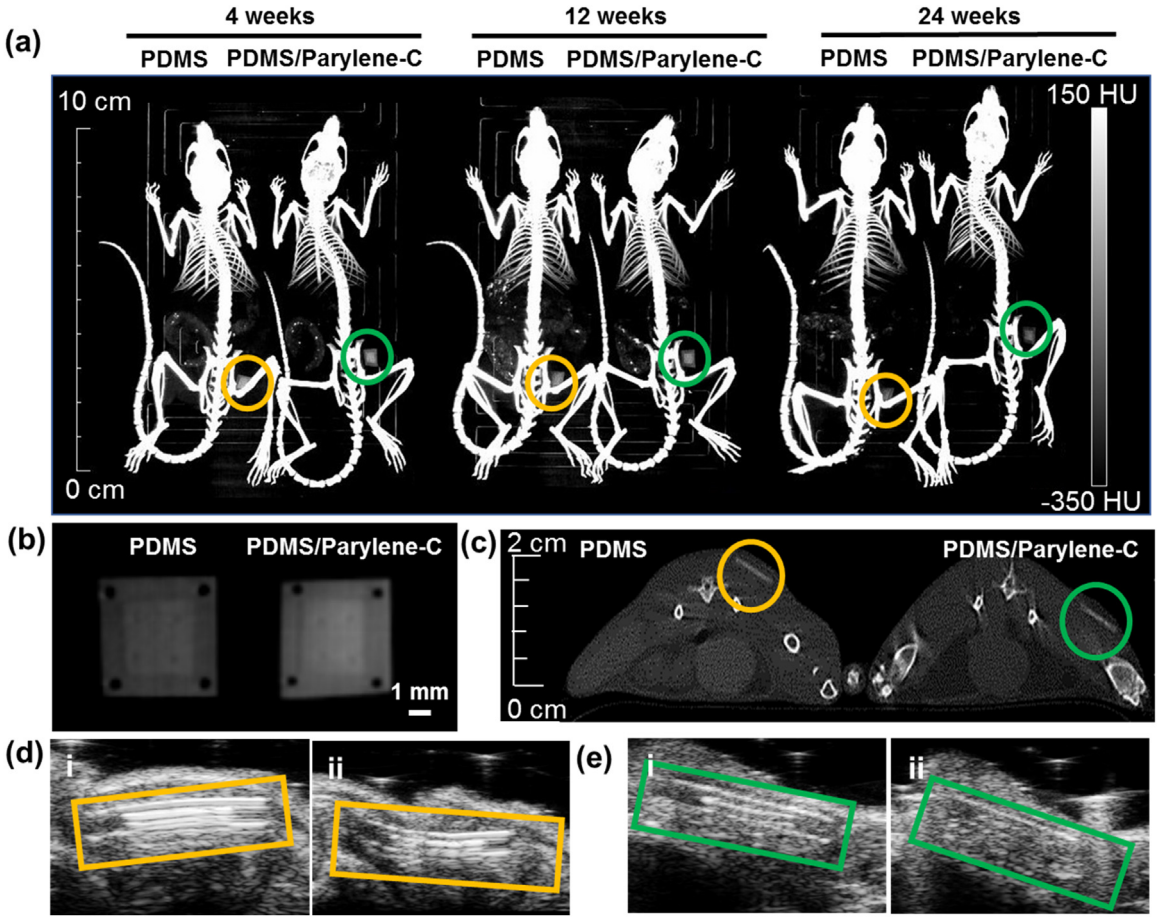

Fig. 2. *In vivo* CT and ultrasound imaging of i-NGs in ICR mice body. **(a)** CT 3D projection images of ICR mice with NG implanted on the top surface of deep muscle near the hip joint. The mouse on the right- and left-hand-side of each pair was implanted with a i-NG packaged by PDMS (yellow circle) and PDMS/Parylene-C (green circle), respectively. **(b)** Enlarged CT scans of PDMS packaged (left panel) and PDMS/Parylene-C packaged i-NGs (right panel). These devices were obtained after 24 weeks of implantation and cleaned before CT scan. **(c)** CT transverse images of ICR mice at the 12th week post implantation. The left and right images were from mice implanted with i-NGs packaged by PDMS (yellow circle), and PDMS/Parylene-C (green circle), respectively. **(d)** Ultrasound imaging of PDMS packaged i-NGs and the surrounding tissues. Images of static (i) and movement state (ii) were presented. **(e)** Ultrasound imaging of PDMS/Parylene-C packaged i-NGs and the surrounding tissues. Images of static (i) and movement state (ii) were presented.

ultrasound as highlighted by the dashed square boxes. The top and bottom high echo lines represented the two encapsulation layers of the i-NG. Between them, the two short high echo lines represented the two gold electrodes. Several high echo lines below the NG region could be related to multiple reflection artifacts. This ultrasound artifact is typically resulted from the movement of imaging target. When the mice hip muscle was relaxed, the PDMS-encapsulated NG exhibited a slight upward bending toward the skin direction, exactly following the shape of the muscle (Fig. 2d-i); whereas, the NG with Parylene-C exhibited a fairly straight profile (Fig. 2e-i). When the skin near the hip joint was stretched, the deep muscle at the implantation region was elongated. Accordingly, an apparent downward bending was observed from the PDMS-encapsulated NG (left panel of Fig. 2d-ii, supplementary video S2), suggesting that the NG could follow the movement of attached muscle precisely. However, the Parylene-C packaged NG remained a straight profile regardless of the muscle motions (right panel of Fig. 2e-ii, supplementary video S3). This is because Parylene-C has a much higher Young's modulus (3–5 GPa) compared to PDMS (0.1–1 MPa) [36–38], which largely increased the rigidity of the i-NG even when its thickness was relatively small. In order to maximize the i-NG's electrical output, it is critical for the i-NG to show corresponding deflection as the supporting muscle or tissue moves. In this regard, pure PDMS would be a superior packaging material that can provide a desired device flexibility.

Supplementary material related to this article can be found online at doi:10.1016/j.nanoen.2018.07.008.

Pathological analyses of the implanted devices were performed at the 2nd, 4th, 12th, and 24th week after implantation to diagnose the potential infections and necrosis in surrounding tissues. Gross pathology was performed first by reopening the implantation area and examining the i-NGs and its surrounding tissues. There were no signs of toxicity or incompatibility induced by the NG, including changes of shape, color and structure of surrounding tissues (Fig. S7). After 24 weeks of implantation, both i-NGs remained a tight adhesion to the muscle surface and no detachment was observed. Growth of tissues through the pinholes (without stitch) on the encapsulation layer was observable, which further tightened the i-NG on muscle surface. Haematoxylin and Eosin (H&E) staining was used to examine the position, toxicity, and bio-compatibility of the i-NG devices at different time frame. Regional tissues from the skin to deep layer muscle from the implantation location were shown by H&E staining (Fig. 3). Tissue from the same region in ICR mice without implantation was sectioned and stained as well for comparison. Due to the multiple washing steps in the process of H&E staining, the NG piece could not to be preserved; whereas a gap between the adjacent tissue and deep muscle could be observed in each section, indicating the location of the i-NG. The surrounding tissues of the NG exhibited no observable differences compared to the sham sample. There were no obvious infiltrations of lymphocytes in the adjacent tissues including skin, tissue and muscle layers. Neither tissue injury nor morphological change at muscular cells were found. No signs of cellular toxicity or muscular atrophy/degeneration were observed over that 24-week period. In general, histological analysis revealed no signs of toxicity or incompatibility induced by both PDMS and Parylene-C packaged NGs, confirming the good bio-compatibility of our i-NGs over a long testing period.

To determine the physiological and biochemical states of whole body functions of the mice, blood and serum test were performed at the same implantation time frames, *i.e.* 2, 4, 12, and 24 weeks after implantation. Fig. 4 summarizes all the tested factors where the normal range is marked between two violet dashed lines. First of all, the inflammation-related factors including lymphocytes (LYM), white blood cells (WBC), monocytes (MON), neutrophile granulocyte (NEU) and neutrophile granulocyte percentage (NEU percentage) did not show any abnormality, which further confirmed that there was no inflammation in the entire body over 6 months of NG implantation. The implanted NGs did not induce any abnormal readings of the number of red blood cells (RBC) and hemoglobin (HGB), confirming no signs of anemia. Normal blood urea nitrogen (BUN) and serum creatinine (SCr) suggested normal renal function, and normal aspartate transaminase (AST) and alanine transaminase (ALT) suggested normal liver function during the entire 6-month implantation period. The only abnormal reading shown in the blood test was platelets (PLT). PLT showed a high reading during the first two weeks of implantation. As a component of blood, PLT functions along with the coagulation factors to stop bleeding by clumping and clotting blood vessel injuries [39]. As a result, a temporarily increased PLT number is usually considered as a common situation related to post-surgery coagulation [40]. The PLT number decreased gradually over longer time and eventually reached the normal

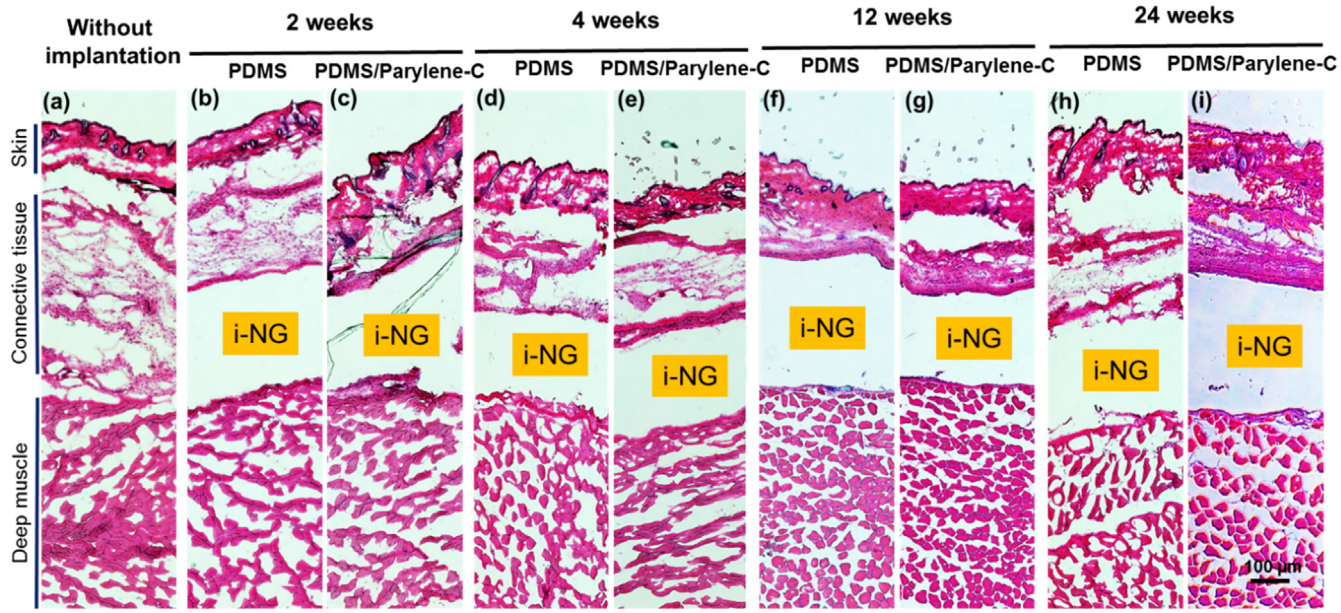

Fig. 3. H&E staining of regional tissue from skin to deep layer muscle. Sham sample from a mouse without implantation **(a)** and sliced samples from mice implanted with PDMS- and PDMS/Parylene-C-packaged NGs for 2 weeks **(b and c)**, 4 weeks **(d and e)**, 12 weeks **(f and g)**, and 24 weeks **(h and i)**, respectively. A gap between connective tissue and deep muscle was found in each mouse, which indicated the location of the i-NG.

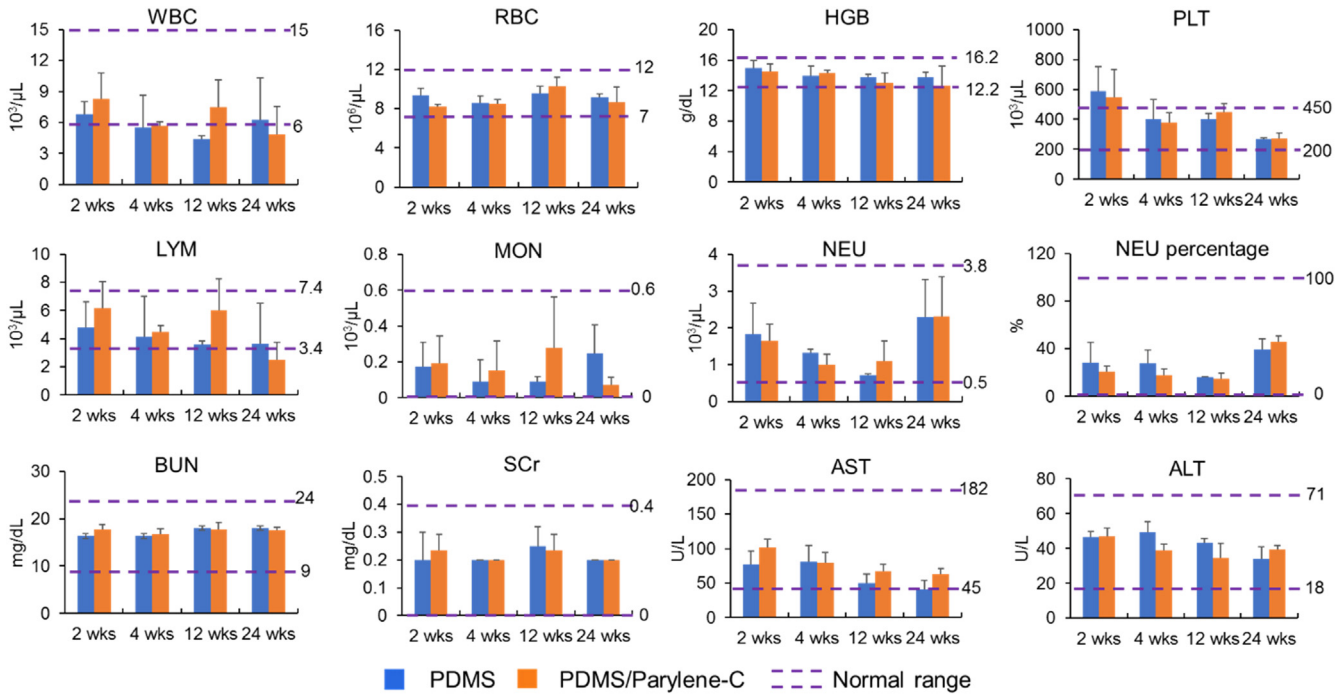

Fig. 4. Periodical blood and serum test results. Blue and orange bars represented i-NGs packaged with PDMS and PDMS/Parylene-C, respectively. The normal range is marked in between two violet dashed lines. The inflammation factors including white lymphocytes (LYM), blood cells (WBC), monocytes (MON), neutrophile granulocyte (NEU) and neutrophile granulocyte percentage (NEU percentage). The red blood cells (RBC) and hemoglobin (HGB) were related to anemia. For other remaining values, the blood urea nitrogen (BUN), serum creatinine (SCr) are correlated to kidney function while aspartate transaminase (AST) and alanine transaminase (ALT) are linked to liver function. The changes of platelets (PLT) represented the coagulation function after surgery.

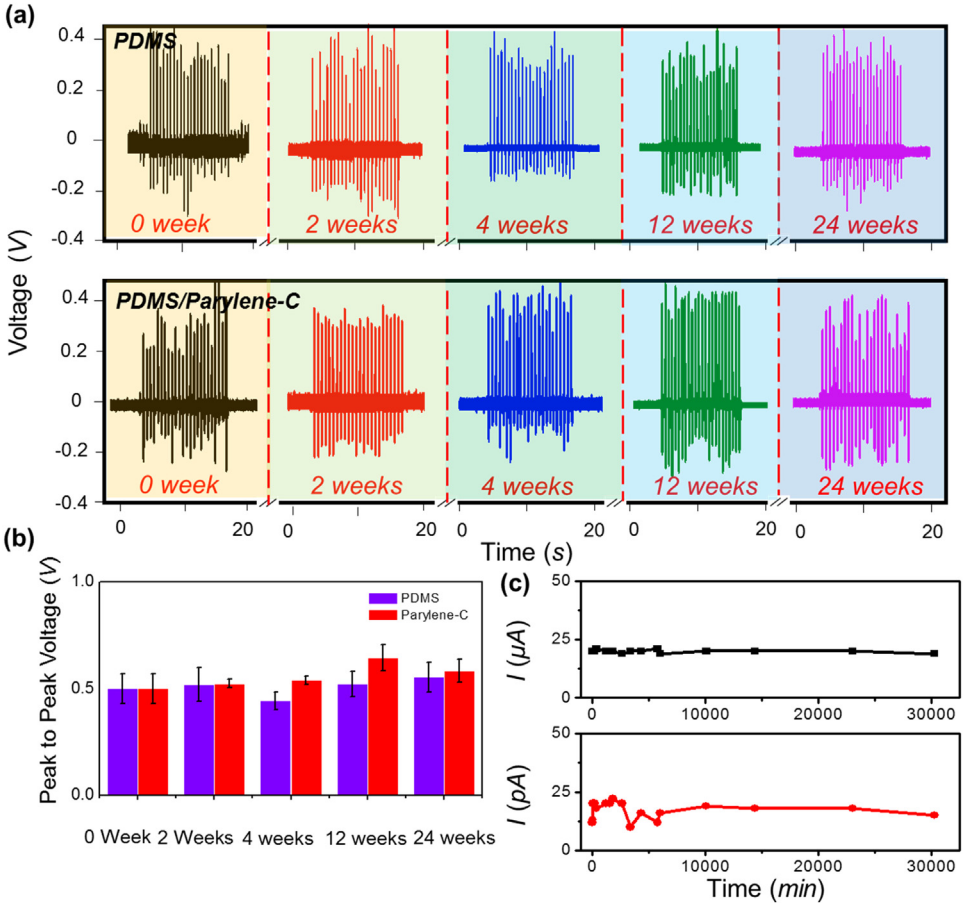

Fig. 5. I-NG performance stability investigation. **(a)** *In vitro* voltage outputs of PDMS and PDMS/Parylene-C packaged i-NGs after they were taken out from sacrificed mice at different time frames. **(b)** Stability of voltage outputs as a function of time for i-NGs with different packaging strategies. The purple and red bars represent i-NGs with PDMS and PDMS/Parylene-C package, respectively. **(c)** Leakage current test of PDMS-package NGs over 21 days. Upper figure is the input current signal (provided by the function generator). Bottom figure is the corresponding leakage current measured between the NG surface and ground.

range when the i-NGs were implanted more than 6 weeks. In general, no significant abnormal readings were detected from the blood and serum test, which further confirmed that both PDMS and Parylene-C packaged i-NGs had excellent biocompatibility over a long period of time.

3.3. Long-term electrical performance evaluation

Biofluid is one of the chemically harsh environments which pose threats to biomedical implants by eroding the packaging layer, reacting with the functional components, and leading to device failure. While above investigation confirmed the excellent bio-compatibility of the selected packaging materials, it is equally important to confirm that the i-NG can be fully protected from the erosive bio-environment and remain an un-affected performance during the long-term implantation. In addition, the protective package also needs to provide electrical insulation, so as to minimize the stray current and thus electrical influences to surrounding tissues. To discover the electrical performance of the encapsulated NGs, the piezoelectric voltage outputs and stray current of all i-NGs were tested as a function of implantation time.

Since it was not practical to monitor the voltage output of implanted i-NG *in vivo* over a long time on living mice, the performance of i-NG was evaluated *in vitro* after a certain period of time of implantation with the hypothesis that *in vitro* output data validate normal *in vivo* operation. This hypothesis was supported by measuring the *in vivo* output of the implanted i-NG and establishing the relationship with *in vitro* data from the same device. When implanted, the i-NG generates a peak-to-peak voltage of ~ 0.05 V when the leg muscle of mouse was stretched at a frequency of 1 Hz; and the voltage raised to ~ 0.1 V at a higher stretching frequency of 2 Hz (Fig. S8). The i-NG yielded ~ 0.3 V piezoelectric output under *in vitro* measurements due to much more significant displacement. This comparison validated *in vitro* characterization was able to justify appropriate *in vivo* function of i-NGs. Piezoelectric voltage outputs were then tested from implanted i-NGs when they were removed from the mice body after 2, 4, 12, and 24 weeks of implantation. All the i-NGs were tested by applying a compressive force of 6 N toward the NG surface at a frequency of 2 Hz. A same NG before implantation was also examined under the same conditions as a reference (marked as 0 week). As shown in Fig. 5a, all the PDMS and Parylene-C packaged i-NGs exhibited a similar peak-to-peak output voltage of ~ 0.5 V. By recording the output constantly over a relatively long time, the average voltage outputs were obtained as a function of implantation time and plotted in Fig. 5b. No trend of voltage amplitude decay could be observed from the data collected during the 24 weeks of implantation period. The steady *in vitro* voltage outputs evidenced the excellent durability of both packaging materials as well as the PVDF films after being placed in a real biological environment and being subjected to constant body motions over a long period of time.

The stray current of i-NGs in biofluids was estimated *in vitro* by immersing a specially-designed NG model in a 0.9% NaCl saline solution for 21 days. During the testing period, a function generator was used to provide a continuous sinusoidal electrical signal toward electrode to simulate the piezoelectric output. The simulated electrical signal remained a 20 μA peak-to-peak current amplitude, which was among the highest current outputs that a piezoelectric NG could produce [41–43]. Selecting such a high output current would ensure the safe operation of all piezoelectric i-NGs with an acceptable-level of stray current. The current signal between the packaging material and ground was monitored as the stray current (the characterization setup is schematically shown in Fig. S9a). The measured stray current shared the same pattern as the function current but with a pA-level amplitude (Fig. S9b). The input current and leakage current were plotted as a function of time in Fig. 5c. The stray current remained at an extremely low level of ~ 20 pA over the entire testing period. This value was only 0.0001% of the functional current, which was at the same level of other reported stray currents of PDMS package [44]. Such a small ratio of stray current of PDMS packages ensured that the i-NG could operate safely inside human body without introducing any detrimental electrical influences to the surrounding tissues.

4. Conclusion

In summary, this work systematically studied the long-term biocompatibility and bio-safety of PVDF-based piezoelectric NGs in female ICR mice, as well as the stability of materials functionality in biological environment. The embedded i-NGs were characterized by multiple advanced *in vivo* imaging techniques, including CT, ultrasound, and photoacoustic. During the 24-month implantation period, the i-NGs were remained at the same subcutaneous region by effective sutures. With the robust protection of encapsulation layers, the device integrity including PVDF film functionality and electrode coverage was well preserved. No signs of toxicity or incompatibility induced by the packaged NGs were observed in the surrounding tissues. Physiological and biochemical states of the whole body functions of the mice remained normal with the implantation of i-NGs during the six-month testing period. Moreover, no reduction in electrical outputs was found over the entire implantation period. Only extremely low stray current was detected from the packaged NG in saline solutions, ensuring an electrically safe operation of the NGs in biological environment. These systematic studies confirmed the long-term biocompatibility and bio-safety of PVDF-based i-NGs, providing a cornerstone for practical i-NG system implantation.

Acknowledgements

J. Li and L. Kang contribute equally to this work. This work was primarily supported by the National Institutes of Health (R01EB021336). J.J.J. and W.C. thank the support from the National Institutes of Health (P30CA014520). L.K. thanks the support from the Beijing Nova Program (Z171100001117024).

Appendix A. Supporting information

Supplementary data associated with this article can be found in the online version at doi:10.1016/j.nanoen.2018.07.008.

References

[1] Z.L. Wang, J.H. Song, Science 312 (2006) 242–246.
[2] X. Wang, J. Song, J. Liu, Z.L. Wang, Science 316 (2007) 102–105.
[3] Z.L. Wang, ACS Nano 7 (2013) 9533–9557.
[4] Z.L. Wang, J. Chen, L. Lin, Energy Environ. Sci. 8 (2015) 2250–2282.
[5] U. Khan, T.H. Kim, H. Ryu, W. Seung, S.W. Kim, Adv. Mater. 29 (2017).
[6] M. Wang, W. Li, C. You, Q. Wang, X. Zeng, M. Chen, RSC Adv. 7 (2017) 6772–6779.
[7] Z. Li, G. Zhu, R. Yang, A.C. Wang, Z.L. Wang, Adv. Mater. 22 (2010) 2534–2537.
[8] M. Parvez Mahmud, N. Huda, S.H. Farjana, M. Asadnia, C. Lang, Adv. Energy Mater. 8 (2018) 1701210.
[9] J. Li, X. Wang, APL Mater. 5 (2017) 073801.
[10] C.L. Sun, J. Shi, D.J. Bayerl, X.D. Wang, Energy Environ. Sci. 4 (2011) 4508–4512.
[11] C. Dagdeviren, B.D. Yang, Y. Su, P.L. Tran, P. Joe, E. Anderson, J. Xia, V. Doraiswamy, B. Dehdashti, X. Feng, B. Lu, R. Poston, Z. Khalpey, R. Ghaffari, Y. Huang, M.J. Slepian, J.A. Rogers, Proc. Natl. Acad. Sci. USA 111 (2014) 1927–1932.
[12] D.H. Kim, H.J. Shin, H. Lee, C.K. Jeong, H. Park, G.T. Hwang, H.Y. Lee, D.J. Joe, J.H. Han, S.H. Lee, Adv. Funct. Mater. (2017).
[13] Q. Zheng, B. Shi, F. Fan, X. Wang, L. Yan, W. Yuan, S. Wang, H. Liu, Z. Li, Z.L. Wang, Adv. Mater. 26 (2014) 5851–5856.
[14] C. Dagdeviren, Z. Li, Z.L. Wang, Annu. Rev. Biomed. Eng. 19 (2017).
[15] Y. Ma, Q. Zheng, Y. Liu, B. Shi, X. Xue, W. Ji, Z. Liu, Y. Jin, Y. Zou, Z. An, W. Zhang, X. Wang, W. Jiang, Z. Xu, Z.L. Wang, Z. Li, H. Zhang, Nano Lett. 16 (2016) 6042–6051.
[16] X.L. Cheng, X. Xue, Y. Ma, M.D. Han, W. Zhang, Z.Y. Xu, H. Zhang, H.X. Zhang, Nano Energy 22 (2016) 453–460.
[17] Q. Zheng, H. Zhang, B. Shi, X. Xue, Z. Liu, Y. Jin, Y. Ma, Y. Zou, X. Wang, Z. An, W. Tang, W. Zhang, F. Yang, Y. Liu, X. Lang, Z. Xu, Z. Li, Z.L. Wang, ACS Nano 10 (2016) 6510–6518.
[18] G. Murillo, A. Blanquer, C. Vargas-Estevez, L. Barrios, E. Ibáñez, C. Nogués,

J. Esteve, Adv. Mater. (2017).
[19] Y. Jin, J. Seo, J.S. Lee, S. Shin, H.J. Park, S. Min, E. Cheong, T. Lee, S.W. Cho, Adv. Mater. 28 (2016) 7365–7374.
[20] Q. Zheng, Y. Zou, Y. Zhang, Z. Liu, B. Shi, X. Wang, Y. Jin, H. Ouyang, Z. Li, Z.L. Wang, Sci. Adv. 2 (2016) e1501478.
[21] R. Yang, Y. Qin, L. Dai, Z.L. Wang, Nat. Nanotechnol. 4 (2009) 34–39.
[22] R. Yang, Y. Qin, C. Li, G. Zhu, Z.L. Wang, Nano Lett. 9 (2009) 1201–1205.
[23] J. Zhou, Y. Gu, P. Fei, W. Mai, Y. Gao, R. Yang, G. Bao, Z.L. Wang, Nano Lett. 8 (2008) 3035–3040.
[24] Y. Yu, H. Sun, H. Orbay, F. Chen, C.G. England, W. Cai, X. Wang, Nano Energy 27 (2016) 275–281.
[25] C.K. Jeong, J.H. Han, H. Palneedi, H. Park, G.-T. Hwang, B. Joung, S.-G. Kim, H.J. Shin, I.-S. Kang, J. Ryu, APL Mater. 5 (2017) 074102.
[26] C.K. Jeong, C. Baek, A.I. Kingon, K.I. Park, S.H. Kim, Small 14 (2018) 1704022.
[27] Z. Zhang, C. Yao, Y. Yu, Z. Hong, M. Zhi, X. Wang, Adv. Funct. Mater. 26 (2016) 6760–6765.
[28] Y. Mao, P. Zhao, G. McConohy, H. Yang, Y. Tong, X. Wang, Adv. Energy Mater. 4 (2014).
[29] D. Güven, J.D. Weiland, M. Maghribi, J.C. Davidson, M. Mahadevappa, R. Roizenblatt, G. Qiu, P. Krulevitz, X. Wang, L. LaBree, Exp. Eye Res. 82 (2006) 81–90.
[30] C. Heo, H. Park, Y.-T. Kim, E. Baeg, Y.H. Kim, S.-G. Kim, M. Suh, Sci. Rep. 6 (2016) 27818.
[31] M. Tohfafarosh, A. Sevit, J. Patel, J.W. Kiel, A. Greenspon, J.M. Prutkin, S.M. Kurtz, J. Long.-Term. Eff. Med. Implants 26 (2016).
[32] Y. Zi, H. Guo, Z. Wen, M.-H. Yeh, C. Hu, Z.L. Wang, ACS Nano 10 (2016) 4797–4805.
[33] Y.-M. Choi, M.G. Lee, Y. Jeon, Energies 10 (2017) 1483.
[34] E. J. Fine, L. Herbst, L. A. Jelicks, W. Koba, D. Theele, Presented at Seminars in Nuclear Medicine 2014.
[35] L.V. Wang, J. Yao, Nat. Methods 13 (2016) 627–638.
[36] T.A. Harder, T.-J. Yao, Q. He, C.-Y. Shih, Y.-C. Tai, Micro Electro Mechanical Systems. in: Proceedings of the Fifteenth IEEE International Conference on, IEEE 2002, pp. 435–438.
[37] D. Fuard, T. Tzvetkova-Chevolleau, S. Decossas, P. Tracqui, P. Schiavone, Microelectron. Eng. 85 (2008) 1289–1293.
[38] D. Wright, B. Rajalingam, J.M. Karp, S. Selvarasah, Y. Ling, J. Yeh, R. Langer, M.R. Dokmeci, A. Khademhosseini, J. Biomed. Mater. Res. Part A 85 (2008) 530–538.
[39] K.R. Machlus, J.N. Thon, J.E. Italiano Jr., Br. J. Haematol. 165 (2014) 227–236.
[40] D.B. Brewer, Br. J. Haematol. 133 (2006) 251–258.
[41] J. Kim, J.H. Lee, H. Ryu, J.H. Lee, U. Khan, H. Kim, S.S. Kwak, S.W. Kim, Adv. Funct. Mater. (2017).
[42] S.-H. Shin, Y.-H. Kim, M.H. Lee, J.-Y. Jung, J. Nah, ACS Nano 8 (2014) 2766–2773.
[43] G.T. Hwang, V. Annapureddy, J.H. Han, D.J. Joe, C. Baek, D.Y. Park, D.H. Kim, J.H. Park, C.K. Jeong, K.I. Park, Adv. Energy Mater. 6 (2016).
[44] A.V. Nurmikko, J.P. Donoghue, L.R. Hochberg, W.R. Patterson, Y.-K. Song, C.W. Bull, D.A. Borton, F. Laiwalla, S. Park, Y. Ming, Proc. IEEE 98 (2010) 375–388.

Jun Li received his B.E. degree in Materials Science and Engineering at Zhejiang University, China in 2016. He is now a Ph.D. student of Materials Science and Engineering at University of Wisconsin-Madison under the supervision of Prof. Xudong Wang since September 2016. His current research interests focus on the nanogenerator design and innovation for implantable medical system and 3D printing of piezoelectric materials.

Lei Kang is an attending doctor working in the Dept. of Nuclear Medicine, in Peking University First Hospital in Beijing, China. He spent one year as a visiting scholar in Cai lab in the University of Wisconsin-Madison in 2017. As a doctor in nuclear medicine, he serves in clinical nuclear medicine services and in basic applied science in molecular imaging. His research focuses on the development of novel radiolabeled molecular probes and new mechanisms in the diagnosis and therapy of malignant tumors, especially on the small nucleotide probes for tumor imaging.

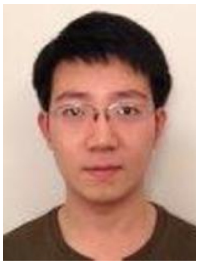

Yanhao Yu received Ph.D. degree of Materials Science and Engineering at the University of Wisconsin-Madison in 2017. His PhD research focuses on the growth and integration of functional oxides, atomic layer deposition, photoelectrochemistry, photovoltaics, nanogenerators and piezotronics. Yanhao joined Joanna Aizenberg group as a postdoctoral fellow at Harvard University in February 2018. His current research centers on structural and surface chemistry tuning of photonic and wetting materials.

Yin Long received her B.S in Electrooptical Engineering and Optical Communication and M.S degree in Optical Engineering at University of Electronic Science and Technology of China, UESTC. She is currently a Ph.D. student of Electro-information Materials and Elements at UESTC while she is also a visiting Ph.D. student at the University of Wisconsin-Madison under the supervision of Prof. Xudong Wang. Her current research focuses on nanogenerator design and piezoelectric nanomaterials synthesis for the application in biomedical engineering.

Justin J. Jeffery has been the manager of small animal imaging facilities since January of 2009. Since 2013, He has managed the daily operations of the University of Wisconsin Carbone Cancer Center (UWCCC) Small Animal Imaging Facility. He is radiation safety certified and certified in the biomethodology of lab rats and mice, and lab animal surgery. He has completed formal coursework in medical imaging physics and nuclear medicine. He also serves as the primary contact and triage person for all new projects and assist UWCCC investigators with experimental design, animal and radiation safety protocol applications.

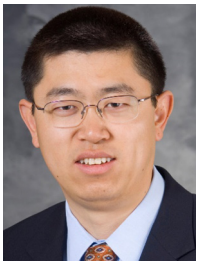

Dr. Cai is a Vilas Distinguished Achievement Professor of Radiology/Medical Physics/Biomedical Engineering/Materials Science & Engineering/Pharmaceutical Sciences at the University of Wisconsin - Madison, USA. He received a PhD degree in Chemistry from UCSD in 2004. Dr. Cai's research at UW-Madison (http://mi.wisc.edu/) is focused on molecular imaging and nanotechnology. He has authored > 270 articles (H-index: 68), edited 3 books, given > 240 talks, and received many awards (*e.g.* Fellow of AIMBE in 2018). Dr. Cai's trainees at UW - Madison have received ~ 100 awards. Dr. Cai has served on the Editorial Board of > 20 journals.

Dr. Xudong Wang is now a Professor and Associate Chair of Materials Science and Engineering at the University of Wisconsin-Madison. He received his Ph.D. degree in Materials Science and Engineering from Georgia Tech in 2005. His current research interests include understanding the coupling effect between piezoelectric polarization and semiconductor functionalities; developing advanced nanomaterials and nanodevices for mechanical energy harvesting from human activities and ambient environment; and studying the growth mechanisms and developing assembly techniques of oxide nanostructures. He is the author of more than 120 publications and holds more than 10 patents on oxide and piezoelectric materials processing and applications.